



Providing Choice & Value

Generic CT and MRI Contrast Agents



**FRESENIUS
KABI**

CONTACT REP

AJNR

**Expanding the Spectrum of Early
Neuroradiologic Findings in β Propeller
Protein-Associated Neurodegeneration**

A. Papandreou, A.K.S. Soo, R. Spaul, K. Mankad, M.A.
Kurian and S. Sudhakar

This information is current as
of July 22, 2025.

AJNR Am J Neuroradiol 2022, 43 (12) 1810-1814

doi: <https://doi.org/10.3174/ajnr.A7693>

<http://www.ajnr.org/content/43/12/1810>

Expanding the Spectrum of Early Neuroradiologic Findings in β Propeller Protein-Associated Neurodegeneration

 A. Papandreou,  A.K.S. Soo,  R. Spaul,  K. Mankad,  M.A. Kurian, and  S. Sudhakar



ABSTRACT

BACKGROUND AND PURPOSE: β propeller protein-associated neurodegeneration (BPAN) is the most common neurodegeneration with brain iron accumulation disorder. Typical radiologic findings are T2 hypointensity in the substantia nigra and globus pallidus, as well as a T1 halolike substantia nigra hyperintense signal surrounding a hypointense central area. However, these findings are often subtle or absent on initial scans, risking diagnostic delay. In this study, we sought to investigate radiologic findings that could aid in the early diagnosis of BPAN.

MATERIALS AND METHODS: A retrospective cohort study was performed in a national referral center, including all pediatric patients with confirmed pathogenic *WDR45* mutations and consistent clinical semiology. MR imaging findings were independently reported by 2 pediatric neuroradiologists.

RESULTS: Fifteen patients were included in the study, and 27 scans were available for review. The initial neuroimaging study was undertaken at a mean age of 3.2 years. Iron deposition was uncommon in patients younger than 4 years of age. Neuroradiologic features from very early on included dentate, globus pallidus, and substantia nigra swelling, as well as a thin corpus callosum and small pontine volume. Optic nerve thinning was also present in all patients.

CONCLUSIONS: Our study highlights the key early MR imaging features of BPAN. Iron deposition in the globus pallidus and substantia nigra is not common in children younger than 4 years of age; clinicians should not be deterred from suspecting BPAN in the presence of the findings described in this study and the appropriate clinical context.

ABBREVIATIONS: BPAN = β propeller protein-associated neurodegeneration; GP = globus pallidus; NBIA = neurodegeneration with brain iron accumulation; SN = substantia nigra

β propeller protein-associated neurodegeneration (BPAN) is emerging as the most common neurodegeneration with brain iron accumulation (NBIA) disorder.¹ It is caused by mutations in *WDR45*, an X-linked gene with a role in early autophagy.^{2,3} Clinically, it typically manifests in infancy with neurodevelopmental delay, epilepsy, autistic-like features, other behavioral issues, stereotypies, and sleep disturbance.

Following a relatively stable course in childhood, BPAN progresses in adolescence or early adulthood with motor regression, dementia, and parkinsonian features.¹⁻³ A core radiologic and neuropathologic hallmark is brain iron accumulation, most prominently in the substantia nigra (SN) but also in the globus pallidus (GP).^{1,3,4} The classically reported MR imaging findings are SN and GP hypointensity on T2-weighted sequences, as well as a halolike SN hyperintensity with a central hypointense band on T1-weighted images.^{3,5,6} Case reports and small cohort studies have described additional BPAN-related findings such as SN swelling, delayed myelination, corpus callosum thinning, deep cerebellar nuclei T2 hyperintensities, and cerebellar atrophy.^{5,7} However, these features are often either absent on initial scans or not specific enough to aid the diagnosis.


BPAN is a rare disease, with an estimated prevalence of 1 in 2–3 million individuals.¹ Due to this rarity and nonspecific clinical presentation at disease onset, the diagnosis is frequently not suspected and only made when nonselective genetic testing (gene

Received August 3, 2022; accepted after revision October 1.

From the Molecular Neurosciences (A.P., A.K.S.S., R.S., M.A.K.), Developmental Neurosciences Programme, Zayed Centre for Research into Rare Disease in Children, University College London Great Ormond Street Institute of Child Health, London, UK; and Departments of Neurology (A.P., A.K.S.S., R.S., M.A.K.) and Neuroradiology (K.M., S.S.), Great Ormond Street Hospital for Children National Health Service Foundation Trust, London, UK.

M.A. Kurian and S. Sudhakar contributed equally to this work.

Please address correspondence to Apostolos Papandreou, MBBS, MRCPCH, PhD, NIHR GOSH BRC Catalyst Fellow, University College London GOS Institute of Child Health, Zayed Centre for Research into Rare Disease in Children, 20c Guilford St, London WC1N 1DZ, UK; e-mail: Apostolos.papandreou@ucl.ac.uk

 Indicates article with online supplemental data.

<http://dx.doi.org/10.3174/ajnr.A7693>

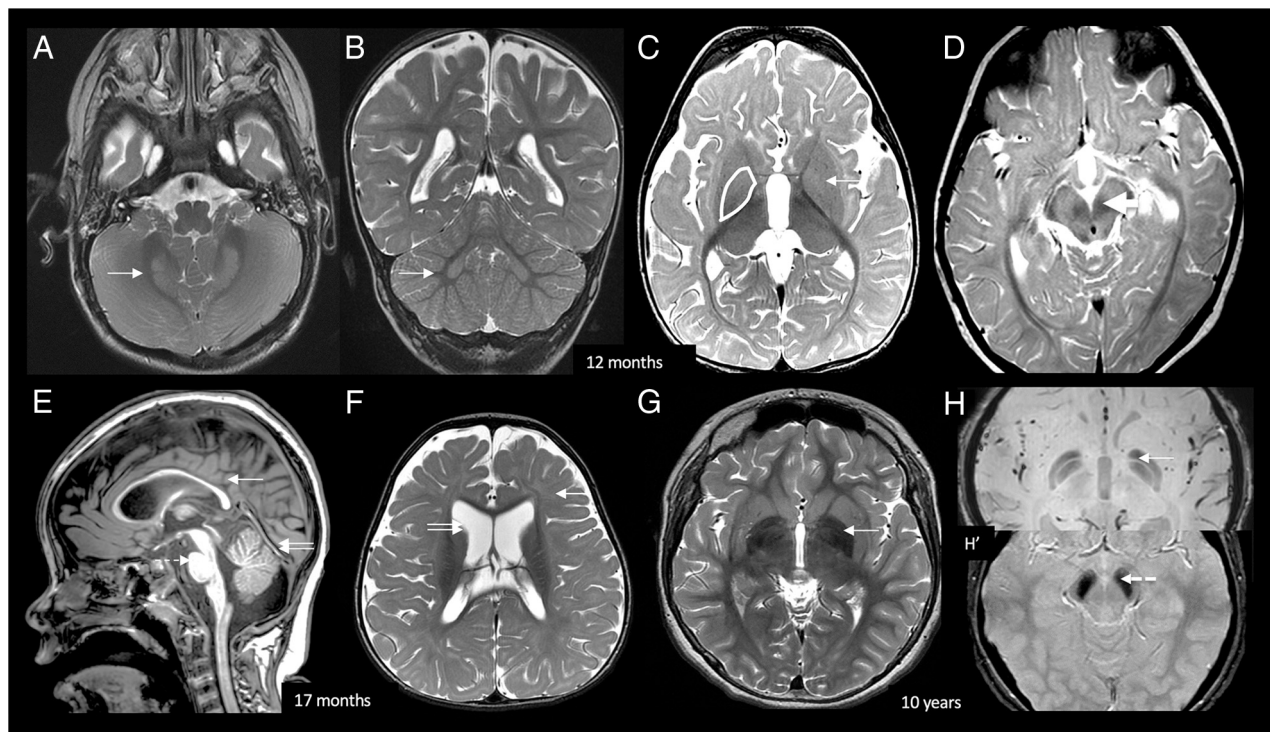


FIG 1. BPAN early radiologic signature. At 12 months of life, axial and coronal T2 (A and B) images show bilateral symmetric dentate nucleus hyperintensity and swelling (white arrows). Axial T2 (C) shows bilateral GP swelling and mild hyperintensity (white arrow). Bilateral SN swelling and T2 hyperintensity are demonstrated on D (white arrow). At 17 months, midsagittal T1 (E) shows diffuse callosal thinning (white arrow), a small pons (dotted arrow), and superior vermal volume loss (double arrow). Axial T2 (F) shows diffuse myelin reduction (white arrow) and prominent lateral ventricles (double arrow). Delayed myelination was infrequently seen in our cohort (1/15 patients). At 10 years of age, T2 axial image (G) in an older child shows GP iron deposition, which is confirmed on SWI (H). H', Increased iron deposition in the SN. The typically reported T1 halo sign was not seen in our pediatric cohort.

panel, exome, or genome sequencing) reveals a *WDR45* pathogenic variant. Prompt establishment of a BPAN diagnosis is crucial for accurate prognosis, genetic counseling, and appropriate multidisciplinary management.¹ Should disease-specific therapies emerge in the future, as has recently happened for many neuro-metabolic conditions,⁸ the need for an accurate diagnosis will become even more pertinent. However, there are currently no BPAN-specific biochemical or early radiologic markers,^{1,9} and genetic variants of unknown significance can be very difficult to interpret.

In this study, we evaluated a cohort of children with BPAN presenting to a single pediatric center and identified several neuroradiologic keys that may facilitate early diagnosis of this disease.

MATERIALS AND METHODS

The study was approved by the Great Ormond Street Hospital Research and Development Audit Department (reference: 3261). All data were anonymized by the lead care teams at the point of collection, so the study did not otherwise require ethics approval.

We undertook a single-center cohort study in patients with an established diagnosis of BPAN attending a UK pediatric neuro-genetic clinic. Inclusion criteria were a disease of childhood onset (0–18 years of life), the presence of a pathogenic *WDR45* genetic variant, and clinical semiology consistent with BPAN. Characterization of the clinical phenotype was undertaken by direct clinical examination and case note review.

Brain MRIs had been performed at either Great Ormond Street Hospital or the referring local hospital and subsequently transferred for neuroradiology review. Different machine models and specifications were used for image acquisition. Brain MRIs were individually reviewed for quality and read by 2 of the authors (K.M. and S.S.), with subsequent discussion for disparate opinions to reach consensus agreement. Specifically, T2-weighted signal intensity and swelling of the dentate nuclei, GP, and SN; T1-weighted signal of the SN; SWI signal changes when available; morphology and size of the brainstem; and the rest of the brain parenchyma were assessed. Optic nerves were also assessed and measured in the prechiasmatic segments on T2- and T1-weighted axial sequences; for this assessment, 3- to 5-mm section-thickness images were used, depending on the availability, while other planes were also used for correct localization. Cerebral and cerebellar atrophy was subjectively graded as mild, moderate, and severe. Cerebellar atrophy was further qualified as vermal (including the gradient, if any), hemispheric, or both. Volumetric analysis was not performed due to insufficient number of cases with volume data. Data were analyzed with descriptive statistics.

RESULTS

Patient Cohort

Sixteen pediatric patients were identified. Some cases have previously been reported (Online Supplemental Data).¹⁰ Neuroimaging was available for 15/16 patients. Mean and median ages at last

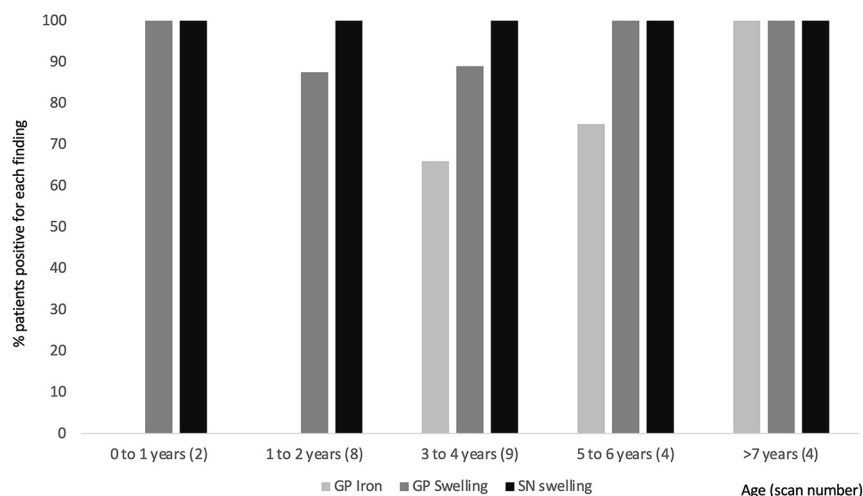


FIG 2. MR imaging findings in relation to age. GP iron deposition is not detectable early on but becomes more prominent after 4 years of age. Conversely, GP and SN swelling are findings present in young patients and persistent later on. GP swelling was absent in 1 patient (B14, 2 scans at 1.5 and 3 years of age) but was otherwise consistently present in all patients and all scans.

clinical review for patients having undergone neuroimaging were 10.5 and 9.95 years, respectively (age range, 3.9–22 years). Mean and median ages at MR imaging were 4.3 and 3 years, respectively. As expected, most (13/15) patients were female. Common clinical manifestations included early infantile-onset developmental delay (15/15), epilepsy (13/15), sleep disturbances (5/15), stereotypies (5/15), and febrile seizures (2/15). Nonstereotypy movement disorders were uncommon, as expected in this age group,¹ with parkinsonian features (1/15), tremor (1/15), dystonia (2/15), and spasticity rarely described.

A single MR imaging brain scan was available for 5/15 cases, whereas 8/15 had 2 scans, and 2/15 had 3 scans in total. Age at scanning ranged from 0.8 to 14 years (mean and median, 3.9 and 3 years, respectively). The first MR imaging was undertaken at a mean age of 3.2 years, whereas the second and third were performed at mean ages of 5.6 and 5.8 years, respectively. The time between follow-up scans ranged from 1.1 to 9.1 years.

Radiologic Findings

Twenty-seven MR imaging scans were available from 15 children (Figs 1–2 and Online Supplemental Data).

First, dentate nucleus abnormalities with T2-weighted hyperintensity and swelling or prominence were seen in 26/27 scans, all except in patient B9 who had only a single scan at 14 years of age.

Regarding the GP, swelling was seen in 26/27 scans, all except in patient B14's second scan at 3 years of age. GP signal T2-hyperintensity was observed in 11/27 scans but mostly in the younger age groups (oldest age at scan: 5 years 5 months of age). In children older than 5 years of age, the GP was either isointense or hypointense compared with the striatum and red nucleus. T1-weighted hyperintensity of the GP was appreciated on only 1 scan at 14 years of age.

Examination of the SN revealed swelling in 22/27, with T2-weighted hyperintensity in 14/27 cases and T2-weighted

hypointensity in 12/27. SN hyperintensity was more common at a younger age (ie, evident in all MR images of children younger than 2 years of age), whereas hypointensity was more prevalent in older patients (ie, in all scans of patients older than 6 years of age). On T1-weighted imaging, SN central hyperintensity was seen in 10/27, whereas peripheral hyperintensity was only present in 1/27 scans at 5 years of age. Progressive findings suggestive of SN iron accumulation, such as evolving T2-weighted hypointensity and T1-weighted central hypointensity with or without peripheral hyperintensity, were evident in 5/15 follow-up scans. The typically reported “T1 halo” sign was not seen in our cohort.

SWI sequences were available in 19/27 scans. Features consistent with iron deposition (eg, hypointensity in minimum-intensity projection algorithm images¹¹) were seen in 12/19 scans, the earliest noted in a patient (B06) at 3 years of age (range, 3–14 years; mean age, 6.8 years; median, 6 years). All cases with features consistent with GP iron deposition (12/19) also showed SN iron deposition. Moreover, iron deposition was not detectable by SWI in early childhood (only evident in 2/12 children younger than 4 years of age, and in 2/15 scans in this age group overall). Conversely, iron was seen on SWI in 6/7 patients (7/8 scans total) imaged at 5 years of age or older. When we compared the GP and SN, the SWI hypointensity was not obviously more prominent in either region. Notably, there were no demonstrable features consistent with iron deposition in the dentate nuclei.

Furthermore, cerebral volume reduction was subjectively seen in 23/27 scans; it was mild in 14/27 (mean age, 4.7 years) and moderate in 9/27 (mean age, 3.6 years) scans. Bicaudate ratio measurements were often high (97th percentile or higher for age and sex¹² in 22/27 scans), confirming the above subjective findings and indicating subcortical WM atrophy (Online Supplemental Data).¹³ Progression of cerebral volume reduction was seen in 1 child (B08, age at the first, second, and third imaging was 3, 6.5, and 7.5 years, respectively). Corpus callosum thinning was evident in all (27/27) patients; this was mainly diffuse but sometimes with body and posterior predominance. Cerebellar atrophy was subjectively seen in 24/27 scans (13/15 patients); it was mild in 15/27 scans, moderate in 9/27 scans, and progressive in 1 of the 11 children (B08) who had serial imaging. The volume reduction was restricted to the superior vermis and superior aspect of the hemispheres in all cases.

Brainstem findings included a small midbrain (less than the first percentile) in all (27/27) scans; a small pons (10th percentile or smaller) in 13/27; and relatively large medulla (75th percentile or larger) in 19/27 scans, compared with reference ranges for age and sex (Online Supplemental Data).¹² In all 27 scans, claval measurements were between 4 and 5 mm; claval prominence was evident in 6/27 scans.

Optic nerve measurements in prechiasmatic segments were lower than the mean expected for age¹⁴ in all children (0–18 months: mean 1.76 mm; 1.5–3 years: mean, 1.8 mm; older than 3 years: mean 2 mm; reference: mean values 2.92 mm, 3.08 mm, >3.2 mm, respectively).

Finally, infrequent MR imaging findings consisted of reduced myelination^{15,16} (patient B07, age 1.3 and 5.4 years at first and second scanning, respectively), large cerebellum (patient B04), and hippocampal sclerosis (patient B14) ($n = 1$ child, each). CT was available in 3 children and showed no pallidonigral calcification (data not shown).

DISCUSSION

BPAN is an X-linked progressive neurodegenerative condition characterized by brain iron accumulation across time; it initially manifests with nonspecific clinicroadiologic features, including absence of iron accumulation in the basal ganglia. Here, we sought to establish an early neuroradiologic signature that could prompt physicians to consider a diagnosis of BPAN. For this purpose, we analyzed MR imaging findings from a pediatric BPAN cohort; to our knowledge, this is the largest single-center pediatric BPAN neuroradiologic study to date.

First, we confirmed the existing literature data that radiologic features consistent with brain iron accumulation were not commonly detectable in early childhood.^{1,5–7} Features of iron deposition were evident in only 2 children younger than 4 years of age (2/15 scans performed at this age) but were seen on SWI in 6/7 patients (7/8 scans total) imaged at 5 years of age or older. Moreover, typically reported findings of T2-weighted GP/SN hypointensity and T1-weighted SN hyperintensity only evolved in a minority of children (and mostly when there were large intervals between follow-up scans). The typically associated hyperintense halo sign was not seen in our cohort.

Conversely, findings present in early disease and in almost all scans analyzed included dentate, GP, and SN T2-weighted hyperintensities and swelling; optic nerve thinning; as well as cerebral and cerebellar atrophy. Delayed myelination was only rarely evident (1/15 patients, consistent with other studies suggesting abnormal myelination in only a minority of patients [28%]).⁶ Additionally, other case reports and small case cohort studies (≤ 4 patients) have also reported GP, SN, and deep cerebellar nuclei T2 hyperintensity and swelling in BPAN, which can be transient and possibly related to pyrexia and seizures.^{5,17} In our cohort, these features tended to persist, with reversal of GP swelling in only 1/11 patients with follow-up imaging.

Although individually nonspecific, the constellation of these neuroimaging findings in the appropriate clinical background is highly suggestive of BPAN, which should be suspected. However, similar findings have recently been reported in patients with biallelic *WIPI2* mutations.¹⁸ Most interesting, *WIPI2* and *WDR45* (also known as *WIPI4*) both belong in the family of WD-repeat proteins interacting with phosphoinositides (WIPI) and have an essential role in the early stages of autophagy.¹⁹ Hence, it would be interesting to see whether similar radiologic patterns emerge in other congenital disorders of autophagy in the future. Moreover, the differential diagnosis should also include other infantile

epileptic encephalopathies, other NBIA, and mitochondrial disorders.^{20,21}

From a pathophysiologic perspective, it is unclear why GP and SN swelling and T2 hyperintensity predominate early on, with iron deposition becoming obvious at a later age. *WDR45* has a role in early autophagy, and it has been postulated that dysfunction in the autophagosome-lysosome degradation pathway might lead to chronic inflammatory changes (that might account for the swelling) and gradual iron deposition in susceptible brain areas.⁷ Overall, more research is needed to better understand the underlying mechanisms linking autophagy, iron metabolism, and neurodegeneration in BPAN.

Other radiologic findings typically associated with other NBIA disorders were also evident in our cohort. First, optic thinning was present in all patients across all scans, and optic nerve measurements were less than the mean expected for age in all cases.¹⁴ Optic nerve thinning has previously been associated with other NBIA disorders, but not specifically with BPAN.^{1,22} Moreover, optic atrophy is only rarely reported in BPAN,^{9,23} and visual electrophysiologic testing has not been systematically reviewed. It is possible that these optic nerve abnormalities might contribute to the visual impairment frequently reported in patients with BPAN in the clinic.^{1,3,9} Second, cerebellar atrophy was a prominent feature in >85% of our patients; similar findings have been reported in other studies,^{6,7,17} though at much lower frequency (eg, 23% in 1 study).⁶ Cerebellar atrophy is also a well-defined radiologic feature of other NBIA disorders such as *PLA2G6*-associated neurodegeneration and fatty acid hydroxylase-associated neurodegeneration.²² Finally, claval prominence was encountered in 4/15 cases (6/27 scans), which has not previously been reported in BPAN and is more typically associated with *PLA2G6*-associated neurodegeneration.²² Notably, the claval prominence in our cohort was milder than that seen in *PLA2G6*-associated neurodegeneration. Overall, the findings of optic nerve thinning, claval hypertrophy, and cerebellar atrophy provide interesting radiologic links with other NBIA disorders.^{1,22} More research is warranted to further characterize these links and elucidate the pathophysiologic mechanisms linking BPAN with other NBIA.

CONCLUSIONS

We describe the largest single-center pediatric neuroimaging study in BPAN. We report a distinct early radiologic signature, with dentate, GP, and SN swelling and T2 hyperintensity, a thin corpus callosum, cerebellar atrophy, optic nerve thinning, and a small pontine volume. The early disease neuroradiologic features described in this study, even in the absence of iron accumulation, should prompt clinicians to include BPAN in the differential diagnosis, especially in the appropriate clinical context. Specifically, lack of iron deposition early in the disease course does not negate the validity of a *WDR45* pathogenic variant identified through genetic testing.

Disclosure forms provided by the authors are available with the full text and PDF of this article at www.ajnr.org.

REFERENCES

1. Wilson JL, Gregory A, Kurian MA, et al; BPAN Guideline Contributing Author Group. **Consensus clinical management**

- guideline for beta-propeller protein-associated neurodegeneration. *Dev Med Child Neurol* 2021;63:1402–09 [CrossRef Medline](#)
2. Saitsu H, Nishimura T, Muramatsu K, et al. De novo mutations in the autophagy gene WDR45 cause static encephalopathy of childhood with neurodegeneration in adulthood. *Nat Genet* 2013;45:445–49, 449e1 [CrossRef Medline](#)
 3. Hayflick SJ, Kruer MC, Gregory A, et al. Beta-propeller protein-associated neurodegeneration: a new X-linked dominant disorder with brain iron accumulation. *Brain* 2013;136:1708–17 [CrossRef Medline](#)
 4. Paudel R, Li A, Wiethoff S, et al. Neuropathology of beta-propeller protein associated neurodegeneration (BPAN): a new tauopathy. *Acta Neuropathol Commun* 2015;3:39 [CrossRef Medline](#)
 5. Kimura Y, Sato N, Ishiyama A, et al. Serial MRI alterations of pediatric patients with beta-propeller protein associated neurodegeneration (BPAN). *J Neuroradiol* 2021;48:88–93 [CrossRef Medline](#)
 6. Adang LA, Pizzino A, Malhotra A, et al. Phenotypic and imaging spectrum associated with WDR45. *Pediatr Neurol* 2020;109:56–62 [CrossRef Medline](#)
 7. Russo C, Ardisson A, Freri E, et al. Substantia nigra swelling and dentate nucleus T2 hyperintensity may be early magnetic resonance imaging signs of β -propeller protein-associated neurodegeneration. *Mov Disord Clin Pract* 2019;6:51–56 [CrossRef Medline](#)
 8. Schulz A, Ajayi T, Specchio N, et al. Study of intraventricular cerliponase alfa for CLN2 disease. *N Engl J Med* 2018;378:1898–1907 [CrossRef Medline](#)
 9. Gregory A, Kurian MA, Haack T, et al. Beta-propeller protein-associated neurodegeneration. In: Adam MP, Ardinger HH, Pagon RA, et al. eds. *GeneReviews University of Washington*; 2016
 10. Willoughby J, Duff-Farrier C, Desurkar A, et al. Functional mRNA analysis reveals aberrant splicing caused by novel intronic mutation in WDR45 in NBIA patient. *Am J Med Genet A* 2018;176:1049–54 [CrossRef Medline](#)
 11. Halefoglou AM, Yousem DM. Susceptibility weighted imaging: clinical applications and future directions. *World J Radiol* 2018;10:30–45 [CrossRef Medline](#)
 12. Garbade SF, Boy N, Heringer J, et al. Age-related changes and reference values of bicaudate ratio and sagittal brainstem diameters on MRI. *Neuropediatrics* 2018;49:269–75 [CrossRef Medline](#)
 13. Bermel RA, Bakshi R, Tjoa C, et al. Bicaudate ratio as a magnetic resonance imaging marker of brain atrophy in multiple sclerosis. *Arch Neurol* 2002;59:275–80 [CrossRef Medline](#)
 14. Maresky HS, Ben Ely A, Bartischovsky T, et al. MRI measurements of the normal pediatric optic nerve pathway. *J Clin Neurosci* 2018;48:209–13 [CrossRef Medline](#)
 15. McErlean A, Abdalla K, Donoghue V, et al. The dentate nucleus in children: normal development and patterns of disease. *Pediatr Radiol* 2010;40:326–39 [CrossRef Medline](#)
 16. Barkovich AJ, Raybaud C. *Pediatric Neuroimaging*. 6th ed. Lippincott Williams & Wilkins; 2018
 17. Ishiyama A, Kimura Y, Iida A, et al. Transient swelling in the globus pallidus and substantia nigra in childhood suggests SENDA/BPAN. *Neurology* 2018;90:974–76 [CrossRef Medline](#)
 18. Maroofian R, Gubas A, Kaiyrzhanov R, et al. Homozygous missense WIPI2 variants cause a congenital disorder of autophagy with neurodevelopmental impairments of variable clinical severity and disease course. *Brain Commun* 2021;3:fcab183 [CrossRef Medline](#)
 19. Proikas-Cezanne T, Takacs Z, Donnes P, et al. WIPI proteins: essential PtdIns3P effectors at the nascent autophagosome. *J Cell Sci* 2015;128:207–17 [CrossRef Medline](#)
 20. Gregory A, Hayflick S. Neurodegeneration with brain iron accumulation disorders: overview. In: Adam MP, Everman DB, Mirzaa GM, eds. *GeneReviews University of Washington*, 1993
 21. Saneto RP, Friedman SD, Shaw DW. Neuroimaging of mitochondrial disease. *Mitochondrion* 2008;8:396–413 [CrossRef Medline](#)
 22. Hayflick SJ, Kurian MA, Hogarth P. Neurodegeneration with brain iron accumulation. *Handb Clin Neurol* 2018;147:293–305 [CrossRef Medline](#)
 23. Rathore GS, Schaaf CP, Stocco AJ. Novel mutation of the WDR45 gene causing beta-propeller protein-associated neurodegeneration. *Mov Disord* 2014;29:574–75 [CrossRef Medline](#)